



OPEN

# Squeezing Millimeter Waves through a Single, Nanometer-wide, Centimeter-long Slit

SUBJECT AREAS:  
NANOPHOTONICS AND  
PLASMONICS  
SURFACE PATTERNING  
TERAHERTZ OPTICS

Xiaoshu Chen<sup>1\*</sup>, Hyeong-Ryeol Park<sup>1\*</sup>, Nathan C. Lindquist<sup>2</sup>, Jonah Shaver<sup>1</sup>, Matthew Pelton<sup>3</sup>  
& Sang-Hyun Oh<sup>1</sup>

Received  
7 August 2014

Accepted  
3 October 2014

Published  
24 October 2014

Correspondence and  
requests for materials  
should be addressed to  
S.-H.O. (sang@umn.  
edu)

\* These authors  
contributed equally to  
this work.

<sup>1</sup>Department of Electrical and Computer Engineering, University of Minnesota, Minneapolis, MN 55455 USA, <sup>2</sup>Physics Department, Bethel University, Saint Paul, MN 55112 USA, <sup>3</sup>Department of Physics, University of Maryland, Baltimore County, Baltimore, MD 21250, USA.

We demonstrate broadband non-resonant squeezing of terahertz (THz) waves through an isolated 2-nm-wide, 2-cm-long slit (aspect ratio of  $10^7$ ), representing a maximum intensity enhancement factor of one million. Unlike resonant nanogap structures, a single, effectively infinitely-long slit passes incident electromagnetic waves with no cutoff, enhances the electric field within the gap with a broad  $1/f$  spectral response, and eliminates interference effects due to finite sample boundaries and adjacent elements. To construct such a uniform, isolated slit that is much longer than the millimeter-scale spot of a THz beam, we use atomic layer lithography to pattern vertical nanogaps in a metal film over an entire 4-inch wafer. We observe an increasing field enhancement as the slit width decreases from 20 nm to 2 nm, in agreement with numerical calculations.

Subwavelength apertures and gaps in metal surfaces can tightly localize electromagnetic waves well below the diffraction limit and lead to strong field enhancements<sup>1–8</sup>. Light-matter interactions in nanometer-scale gaps also reveal novel phenomena such as nonlocal electromagnetic effects, optical rectification, and inelastic electron tunneling<sup>9–12</sup>. The prerequisite for fundamental investigation of such phenomena and their practical utilization is reliable, high-throughput fabrication of these gaps, ideally with dimensions down to the single-digit nanometer scale. While electron-beam lithography can be used to pattern nanometer-scale point junctions in thin metal films<sup>13</sup>, it is not practical to extend a point junction into a long and uniform slit through optically thick metal films and to create a dense array of such slits at the wafer scale. Other approaches based on colloidal nanoparticle junctions<sup>14–16</sup> or film-coupled nanoparticles<sup>12,17</sup> allow the formation of sub-nanometer-scale gaps, but do not allow precise control of their shape and arrangement. Furthermore, to fully take advantage of strong light-matter interactions in the technologically important far-infrared and terahertz (THz) regimes, it is necessary to design and construct these nanogap structures over millimeter or centimeter scales to increase the coupling efficiency of long-wavelength radiation energy into the nanogaps.

Recent experiments by other groups showed a field enhancement factor of 800 at 0.2 THz in 40-nm-wide slits<sup>18–20</sup>. The ability to construct even thinner nanogaps along arbitrarily large in-plane geometries at the wafer-scale can tremendously improve the signal-to-noise ratio, throughput, and repeatability for these experiments; a necessity for exploring THz field enhancement of the narrowest slits. In addition, it is desirable to investigate the THz transmission process and the resultant giant field enhancements using an isolated single slit. When arrays of slits are illuminated with a millimeter-sized beam for THz spectroscopy, it is often difficult to separate out optical effects inside the gap from effects due to periodicity.

Extending a nanometer-wide gap into a centimeter-long slit in a metal film requires constructing a device with an aspect ratio exceeding  $10^7$ . To address this challenge, we developed a patterning technology that allows wafer-scale fabrication of vertically-oriented nanogaps, called atomic layer lithography<sup>21,22</sup>. This technique relies on atomic layer deposition (ALD)<sup>23–25</sup> to define the lateral patterning resolution of the nanogaps. Each ALD cycle deposits a 1–2 Å-thick conformal alumina ( $\text{Al}_2\text{O}_3$ ) layer on the vertical sidewalls of patterned metals, enabling Ångström-resolution control of nanogap width. The key strength of atomic layer lithography over electron-beam and FIB lithography is that the critical dimension — the gap width — is decoupled from the pattern size and density. One can thus, in principle, extend nanometer-wide gaps along the contour of arbitrarily large patterns. Another key



strength of the fabrication process is the simplicity with which patterned metals can be planarized using adhesive tape.

Our previous work<sup>22</sup> demonstrated that  $\text{Al}_2\text{O}_3$ -filled gaps with a lateral width as narrow as 1 nm can be produced in a metal film along the contour of sub-millimeter scale rectangle. Here, we push the limit of our patterning and planarization capabilities by demonstrating nanogaps along 2-centimeter-long contours, proving the robustness and scalability of this technique. The production of a centimeter-long metallic nanogap allows us to perform THz time-domain spectroscopy (TDS) through an isolated sub-wavelength slit ( $\lambda/1,000,000$ ) covering only 0.0002% of the cross-sectional area of an incident THz beam (Fig. 1a). In this experiment, the measured THz wave passes exclusively through the single nanometer-wide gap. By examining the transmitted radiation in the far field, we deduce broadband, non-resonant field enhancement inside the nanogap, in agreement with two-dimensional (2D) computational modeling for an infinitely long slit.

## Results

Using atomic layer lithography (Fig. 1b), we fabricated centimeter-long nanoslits. An array of rectangular patterns ( $0.8 \text{ cm} \times 0.1 \text{ cm}$ ; center-to-center spacing = 1 cm, as shown in Fig. 1c) in a gold film (150 nm in thickness with a 3-nm Ti adhesion layer) was first made on a 4-inch Pyrex glass wafer using photolithography, metal deposition, and lift-off. ALD, at  $250^\circ\text{C}$ , was then used to conformally deposit a thin layer of alumina ( $\text{Al}_2\text{O}_3$ ) over the pattern. The alumina

film thickness was precisely defined, with Ångstrom-scale resolution, by the number of ALD cycles (measured deposition rate of  $1.1 \text{ \AA}$  per cycle). A second layer of gold (150 nm) was deposited by directional electron-beam evaporation to fill the pattern and form the nanogap between the first and second metal layer.

After depositing the second metal layer, excess metal must be removed to expose the nanogaps. This type of critical step is typically done through a series of complicated planarization techniques; however, the poor adhesion between noble metals and oxides led us to the simple and effective solution of merely peeling off the excess metal with adhesive tape (Fig. 1b). Many groups have utilized peeling or stripping techniques for patterned metal fabrication. For example, the PEEL process<sup>26</sup> combines soft lithography and lift-off to produce free-standing metal films, while template stripping<sup>27,28</sup> from silicon molds produces ultra-smooth patterned metals. In the case of atomic layer lithography, wafer-scale peeling with adhesive tape (e.g. 3M Scotch<sup>TM</sup> tape) planarizes the vertically oriented nanogap patterns, dramatically simplifying the process flow. Considering that the second metal layer is only 100–200 nm thick and the width of the trench is on the millimeter scale, it would appear that planarization would be difficult. However, as long as we ensure that the tape does not contact the metal inside the trench, by gently applying it without any extra pressure, only the raised portion of the metal layer is removed. We tested structures with various sizes and shapes, and this tape-based planarization process works well for structures with lateral dimensions as large as 1 cm.

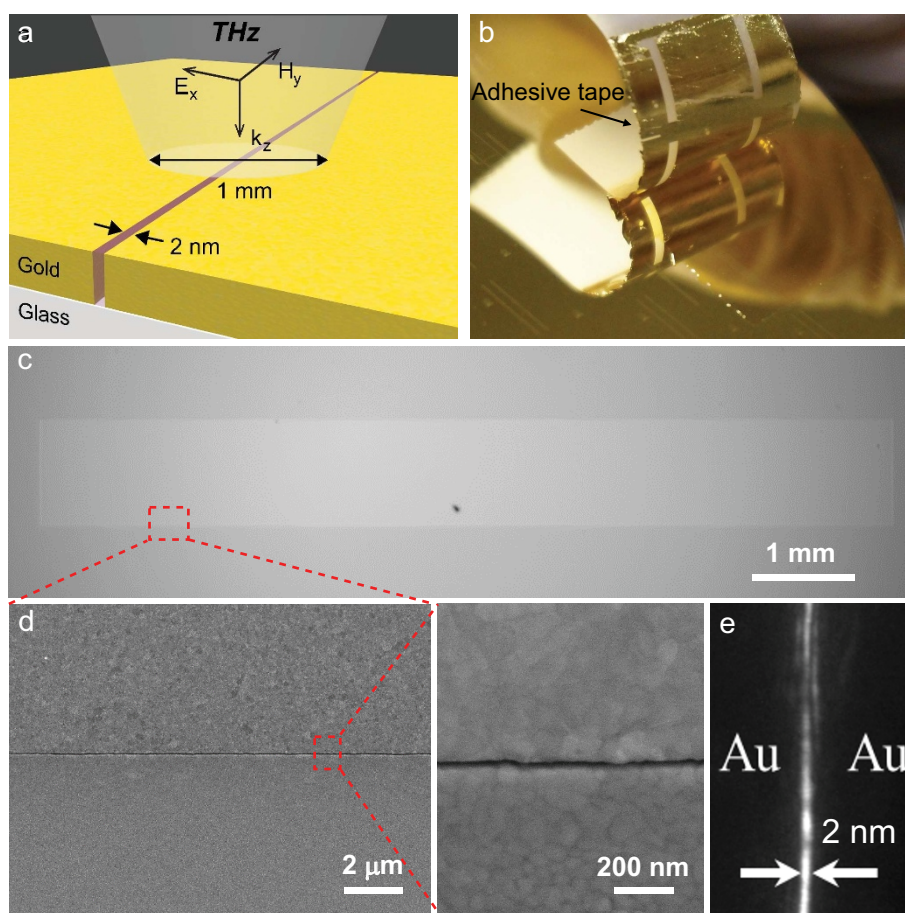


**Figure 1 | Atomic layer lithography of centimeter-scale loop with nanometer-scale gaps.** (a), Illustration of a single, non-resonant nanoslit, one side of the centimeter-scale loop, illuminated at normal incidence by a *p*-polarized, focused THz beam. (b), Photograph of the tape-stripping process to planarize the nanogap patterns. (c), Photograph taken from the back side of the nanogap loop structure ( $0.8 \text{ cm} \times 1 \text{ cm}$ ). (d), Top-view scanning electron micrograph (SEM) of a 20 nm-wide gap in a gold film. (inset) Enlarged SEM image of the left image. (e), Cross-sectional tunneling electron micrograph (TEM) of a 2 nm-wide alumina layer between two gold layers.

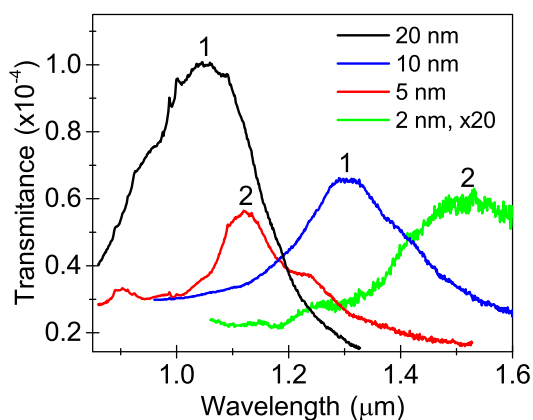


**Figure 2 | Near-infrared (NIR) characterization of cm-long nanoslits in gold films.** Measured transmission spectra through 2, 5, 10, and 20 nm gaps at NIR wavelengths. The transmission peaks of the 2- (green line) and 5-nm (red line) correspond to second-order Fabry-Pérot (FP) resonances. For the 10 and 20 nm gaps, they correspond to first-order FP resonances. The mode orders are indicating by numbers above the spectra.

One part of a long slit with a gap size of 20 nm is shown in the scanning electron microscope image (SEM) in Fig. 1d. For a 2 nm gap, a transmission electron microscope (TEM) was used to confirm the gap size, as shown in Fig. 1e. To confirm that uniform nanogaps are formed through the entire film thickness, we measured optical transmission spectra through the nanoslits. Using near-infrared spectroscopy (see Methods), we observed the first and second order Fabry-Pérot (FP) resonances for different gap sizes (Fig. 2)<sup>5,22,29,30</sup>. As the gap size decreases, the resonances of the same order shift to longer wavelengths. In Fig. 2, we show that, when light with a vacuum wavelength of 1550 nm is confined to a 2 nm gap, it takes on a plasmon wavelength of  $\lambda_{SP} = 149$  nm<sup>5,22,30</sup>, corresponding to an effective refractive index of  $n_{eff} = 10.4$ .

We performed THz time-domain spectroscopy (THz-TDS)<sup>18,31</sup> (see Methods for details) to observe non-resonant transmission of THz waves through single nanoslits in a 150 nm-thick gold film with gap sizes of  $w = 2, 5, 10$ , and 20 nm. To illuminate only one side of the loop (that is, a single, straight slit) with the incident THz wave, we use a 1 mm-by-1 mm aperture in a stainless steel plate. A small but non-negligible direct transmission through the unpatterned gold film is subtracted when estimating the field enhancement in the nanogap<sup>18</sup>. Figure 3a shows the transmitted electric field amplitudes through the nanoslit samples and the unpatterned gold film on the glass substrate.

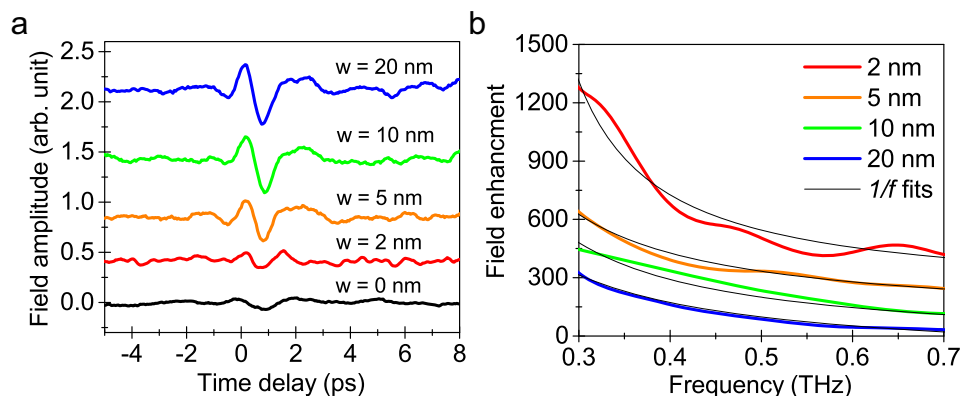


**Figure 3 | Terahertz transmission through a single nanoslit.** (a), Time-domain signals for transmitted THz waves through single nanoslits with gap sizes,  $w = 20, 10, 5, 2$ , and 0 nm (unpatterned). The graphs are offset along the vertical axis. (b), Fourier-transformed electric-field enhancement spectra of the nanoslits in the frequency domain. Black lines indicate  $1/f$  dependence.

Transmitted electric field amplitude spectra were obtained by Fourier-transforming time-domain signals, which were then normalized to the reference signal collected for transmission through the glass substrate. We infer near-field enhancement factors by normalizing the transmitted amplitudes by the slit coverage ratio, according to Kirchhoff diffraction theory<sup>18,32</sup>. This can be done because the minimum slit width of 2 nm is larger than the charge screening length ( $< 1$  nm). Figure 3b shows that the enhancement varies approximately as  $1/f$ , where  $f$  is frequency, over the entire measured spectral range. Previous work showed that the field enhancement increases as the slit width decreases down to tens of nanometers, due to capacitive charge accumulation from light-induced currents at the sidewalls<sup>18–20,33</sup>. Reducing the slit width to 2 nm allowed us to achieve a non-resonant electric field ( $E$ ) enhancement of 1300 at  $f = 0.3$  THz; this corresponds to a maximum intensity ( $|E|^2$ ) enhancement of  $10^6$ , the highest yet obtained in single-slit studies. This enhancement is entirely due to the large ratio between the free-space wavelength of the THz wave and the narrow slit width, and does not rely on any resonant effects. While the enhancement is smaller than that obtained for resonant ring apertures<sup>22,34</sup>; it is highly broadband without any cut-off or interference effects, and is limited only by the frequency response of the metal.

We also carried out two-dimensional finite-element modeling (FEM) using COMSOL to estimate the electric field enhancement as a function of the gap size,  $w$ . (For details of the simulations, see Methods.) In Fig. 4a, the simulated field enhancement factors are in good qualitative agreement with the measured factors, showing capacitor-like  $1/w$  dependence<sup>18,33</sup>. Figure 4b shows a cross-section of the electric field distribution around a 2-nm-wide slit. The enhanced electric field within the gap is nearly constant along its entire thickness. Strongly confined electric fields with enhancement factors over 1,000 near the entrance and exit corners are also observed.

## Conclusions

We produced a wafer-scale array of 2-cm-long and 2-nm-wide gaps through optically thick metal films by combining photolithography, ALD, and tape-based planarization. To demonstrate the utility of these extremely high-aspect-ratio ( $>10^7$ ) nanostructures, single-slit NIR transmission and THz-TDS were performed. Using these measurements we inferred a non-resonant field enhancement factor of 1300 when a millimeter wave passes through a single 2-nm-wide metal slit. As transmission through the gap and the resulting high field enhancements are non-resonant, they will be effective over a broad range of frequencies. The nanogaps could thus be used to enhance wave-mixing processes that involve extremely different frequencies, such as frequency conversion from the visible or NIR to the THz. Placing molecules and nanoparticles inside the gaps will lead to

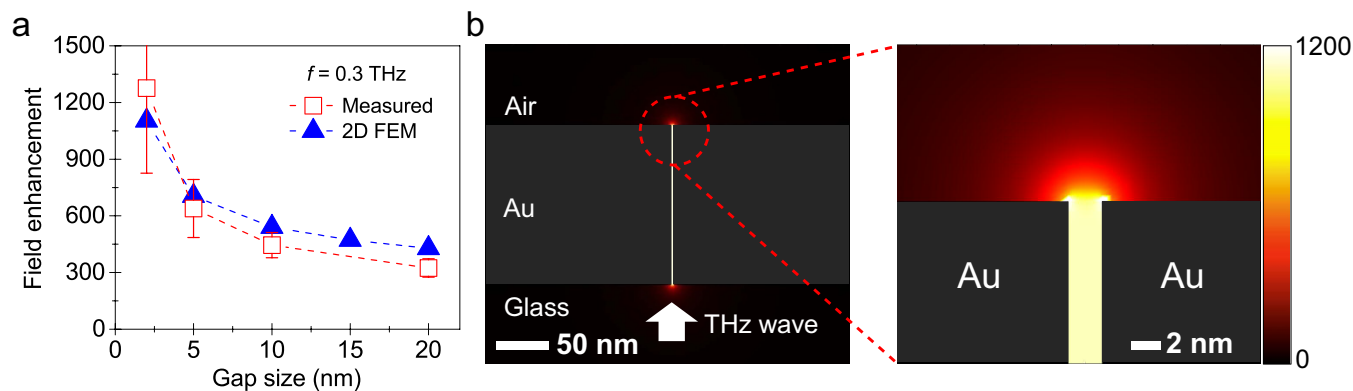


**Figure 4 | Two-dimensional (2D) finite-element simulation of a single nanoslit.** (a), Red squares indicate measured field enhancement of the nanogaps at 0.3 THz as a function of the gap size, performed by THz time-domain spectroscopy. Blue triangles indicate simulated field enhancements by 2D finite-element modeling. (b), (left) Calculated electric field amplitude around a 2-nm-wide slit in a 150-nm-thick gold film. (right) Enlarged electric field amplitude distribution around the exit of the nanoslit. The slit is filled with alumina (Al<sub>2</sub>O<sub>3</sub>).

plasmon-enhanced luminescence; the extended slit length will make it possible to gather statistical data from a large number of single quantum emitters simultaneously. For sensing applications, cm-long nanogaps facilitate integration with a large array of microfluidic channels. Furthermore, by scaling up the loop length and packing density, it may be possible to study resonant transmission of micro-waves through nanogaps<sup>2</sup>.

## Methods

**Nanogap fabrication via atomic layer lithography.** The nanogap is fabricated using the atomic layer lithography method developed in our previous work<sup>22</sup>. First, an array of 0.8 cm × 0.1 cm rectangular patterns in metal films are fabricated on a Pyrex glass substrate using negative resist (NR71-1500P) and photolithography, followed by metal deposition (150 nm Au with Ti adhesion layer) using electron-beam evaporation and lift-off in a solvent (1165 remover). After cleaning with acetone, methanol, and IPA and blowing dry with N<sub>2</sub> gas, the patterned metal film is conformally coated with a thin Al<sub>2</sub>O<sub>3</sub> layer by ALD at 250°C (Cambridge NanoTech Inc., Savannah<sup>TM</sup>). Trimethylaluminum and H<sub>2</sub>O vapor were sequentially pulsed through the ALD chamber and N<sub>2</sub> gas was used to purge the chamber after each injection. The thickness of the Al<sub>2</sub>O<sub>3</sub> film is calibrated using ellipsometry on a Si reference water placed in the same chamber, and the measured deposition rate for Al<sub>2</sub>O<sub>3</sub> is 1.1 Å/cycle. After ALD, the trenches are filled with second metal by directional metal evaporation (Temescal). The metal deposited outside of the trench is easily removed using adhesive tape (single-sided 3M Scotch Magic Tape<sup>TM</sup>) without leaving any residue.

**Electron microscopy sample preparation.** TEM samples are prepared by FIB milling. A thin film of Au/Al<sub>2</sub>O<sub>3</sub>/Au is cut across a nanogap on one side of the rectangular pattern. The lamella is then picked up by an Omniprobe and was attached to a TEM copper grid. The lamella is further thinned with ion beam milling to less than 100 nm, and is imaged in a TEM (FEG-TEM, FEI Tecnai G2 30). For preparation of SEM samples, the top alumina layers on the metal surface are etched using reactive ion etching (RIE) with an inductively coupled plasma (Plasmalab System100 ICP180, Oxford Ltd.), to avoid charging effects. The samples are then imaged in an SEM (FEG-SEM, JEOL 6700).

**Near-infrared spectroscopy.** A broadband fiber-coupled, laser driven light source (Energetiq, EQ-99FC) is used to illuminate single nanogaps through a 600 μm fiber, reflective collimator, polarizer, and condenser on top of an inverted microscope (Nikon Ti-S). Transmitted light is collected with a 50×, 0.9 NA objective and imaged onto the entrance slit of a 300 mm focal length imaging spectrometer (Acton SP2300i) equipped with a thermoelectrically cooled, 256-element InGaAs diode array (BaySpec Nunavut). The imaged nanogap length is 5 μm, and 5 measurements are obtained, for a total length of 25 μm. The incident light polarization is adjusted for maximum throughput (perpendicular to the nanogap contour). Spectra are background subtracted and normalized using the spectrum for direct transmission through the glass substrate.

**Terahertz time-domain spectroscopy.** A terahertz pulse with a few picoseconds pulse width is generated from a GaAs-based photoconductive antenna (Tera-SED, Gigaoptics, GmbH) illuminated by a femtosecond Ti:sapphire laser pulse train with a center wavelength of 780 nm, 80 MHz repetition rate, and 90 fs pulse width (Mai Tai XF, Newport Corporation). The p-polarized terahertz light passes through the nanogap samples at normal incidence and is detected by electro-optic sampling using a 1-mm-thick ZnTe crystal (INGCRYS Laser System Ltd.).

**Two-dimensional Finite-Element Method simulations using COMSOL.** We numerically simulated infinitely long metallic slits with various gap sizes between 2 nm and 20 nm using COMSOL. The Drude model is used to fit the optical parameters of the gold film at THz frequencies (plasma frequency  $1.37 \times 10^4$  THz, damping parameter 40.7 THz)<sup>35</sup>. The gold film has a thickness of 150 nm, and a size-dependent dielectric constant for the Al<sub>2</sub>O<sub>3</sub> layer inside the gap is used<sup>22,36</sup>. Due to the extreme length-scale differences between the millimeter waves and nanometer gaps, care is taken while meshing the simulation area. The largest element size in free space is 20 μm whereas the smallest element size in the gap is 0.1 nm. Perfectly matched layers (PML) are used to minimize boundary reflections with plane-wave THz illumination. The simulation area is 9 mm high and 8 mm wide. Field enhancements within the gap are calculated by comparing the average amplitude within the entire gap thickness to a reference amplitude of the transmitted electric field through a glass/air interface without the nanogap or metal layer. After normalization, there is no difference between field enhancement factors with different incident light directions, i.e. from air to glass or from glass to air.

1. Ebbesen, T. W., Lezec, H. J., Ghaemi, H. F., Thio, T. & Wolff, P. A. Extraordinary optical transmission through sub-wavelength hole arrays. *Nature* **391**, 667–669 (1998).
2. Yang, F. Z. & Sambles, J. R. Resonant transmission of microwaves through a narrow metallic slit. *Phys. Rev. Lett.* **89**, 063901 (2002).
3. Xie, Y., Zakharian, A. R., Moloney, J. V. & Mansuripur, M. Transmission of light through slit apertures in metallic films. *Opt. Express* **12**, 6106–6121 (2004).
4. Bravo-Abad, J., Martin-Moreno, L. & Garcia-Vidal, F. J. Transmission properties of a single metallic slit: From the subwavelength regime to the geometrical-optics limit. *Phys. Rev. E* **69**, 026601 (2004).
5. Miyazaki, H. T. & Kurokawa, Y. Squeezing visible light waves into a 3-nm-thick and 55-nm-long plasmon cavity. *Phys. Rev. Lett.* **96**, 097401 (2006).
6. Adam, A. J. L. *et al.* Advanced terahertz electric near-field measurements at sub-wavelength diameter metallic apertures. *Opt. Express* **16**, 7407–7417 (2008).
7. Garcia-Vidal, F. J., Martin-Moreno, L., Ebbesen, T. W. & Kuipers, L. Light passing through subwavelength apertures. *Rev. Mod. Phys.* **82**, 729–787 (2010).
8. Pendry, J. B., Aubry, A., Smith, D. R. & Maier, S. A. Transformation optics and subwavelength control of light. *Science* **337**, 549–552 (2012).
9. Ward, D. R., Huser, F., Pauly, F., Cuevas, J. C. & Natelson, D. Optical rectification and field enhancement in a plasmonic nanogap. *Nature Nanotechnol.* **5**, 732–736 (2010).
10. Halas, N. J., Lal, S., Chang, W. S., Link, S. & Nordlander, P. Plasmons in strongly coupled metallic nanostructures. *Chem. Rev.* **111**, 3913–3961 (2011).
11. Bharadwaj, P., Bouhelier, A. & Novotny, L. Electrical excitation of surface plasmons. *Phys. Rev. Lett.* **106**, 226802 (2011).
12. Ciraci, C. *et al.* Probing the ultimate limits of plasmonic enhancement. *Science* **337**, 1072–1074 (2012).
13. Duan, H. G., Fernandez-Dominguez, A. I., Bosman, M., Maier, S. A. & Yang, J. K. W. Nanoplasmonics: classical down to the nanometer scale. *Nano Lett.* **12**, 1683–1689 (2012).
14. Michaels, A. M., Jiang, J. & Brus, L. Ag nanocrystal junctions as the site for surface-enhanced Raman scattering of single Rhodamine 6G molecules. *J. Phys. Chem. B* **104**, 11965–11971 (2000).
15. Xu, H. X. & Käll, M. Surface-plasmon-enhanced optical forces in silver nanoaggregates. *Phys. Rev. Lett.* **89**, 246802 (2002).
16. Pelton, M. & Bryant, G. W. *Introduction to metal-nanoparticle plasmonics*, pp 135–161 (John Wiley & Sons, Hoboken, 2013).
17. Ciraci, C. *et al.* Film-coupled nanoparticles by atomic layer deposition: comparison with organic spacing layers. *Appl. Phys. Lett.* **104**, 023109 (2014).



18. Seo, M. A. *et al.* Terahertz field enhancement by a metallic nano slit operating beyond the skin-depth limit. *Nature Photon.* **3**, 152–156 (2009).
19. Shalaby, M. *et al.* Concurrent field enhancement and high transmission of THz radiation in nanoslit arrays. *Appl. Phys. Lett.* **99** (2011).
20. Shalaby, M. *et al.* Skirting terahertz waves in a photo-excited nanoslit structure. *Appl. Phys. Lett.* **104** (2014).
21. Im, H., Lindquist, N. C., Lesuffleur, A. & Oh, S. H. Atomic Layer Deposition of Dielectric Overlayers for Enhancing the Optical Properties and Chemical Stability of Plasmonic Nanoholes. *ACS Nano* **4**, 947–954 (2010).
22. Chen, X. *et al.* Atomic layer lithography of wafer-scale nanogap arrays for extreme confinement of electromagnetic waves. *Nature Commun.* **4**, 2361 (2013).
23. Leskela, M. & Ritala, M. Atomic layer deposition chemistry: Recent developments and future challenges. *Angew. Chem. Int. Ed.* **42**, 5548–5554 (2003).
24. George, S. M. Atomic layer deposition: an overview. *Chem. Rev.* **110**, 111–131 (2010).
25. Lindquist, N. C., Nagpal, P., McPeak, K. M., Norris, D. J. & Oh, S. H. Engineering metallic nanostructures for plasmonics and nanophotonics. *Rep. Prog. Phys.* **75**, 036501 (2012).
26. Henzie, J., Lee, M. H. & Odom, T. W. Multiscale patterning of plasmonic metamaterials. *Nature Nanotechnol.* **2**, 549–554 (2007).
27. Nagpal, P., Lindquist, N. C., Oh, S. H. & Norris, D. J. Ultrasmooth patterned metals for plasmonics and metamaterials. *Science* **325**, 594–597 (2009).
28. Lindquist, N. C., Nagpal, P., Lesuffleur, A., Norris, D. J. & Oh, S. H. Three-Dimensional Plasmonic Nanofocusing. *Nano Lett.* **10**, 1369–1373 (2010).
29. Gordon, R. & Brolo, A. G. Increased cut-off wavelength for a subwavelength hole in a real metal. *Opt. Express* **13**, 1933–1938 (2005).
30. de Waele, R., Burgos, S. P., Polman, A. & Atwater, H. A. Plasmon dispersion in coaxial waveguides from single-cavity optical transmission measurements. *Nano Lett.* **9**, 2832–2837 (2009).
31. Grischkowsky, D., Keiding, S., Vanexter, M. & Fattinger, C. Far-Infrared Time-Domain Spectroscopy with Terahertz Beams of Dielectrics and Semiconductors. *J. Opt. Soc. Am. B* **7**, 2006–2015 (1990).
32. Kyoung, J. S., Seo, M. A., Park, H. R., Ahn, K. J. & Kim, D. S. Far field detection of terahertz near field enhancement of sub-wavelength slits using Kirchhoff integral formalism. *Opt. Commun.* **283**, 4907–4910 (2010).
33. Kang, J. H., Kim, D. S. & Park, Q. H. Local Capacitor Model for Plasmonic Electric Field Enhancement. *Phys. Rev. Lett.* **102**, 093906 (2009).
34. Shu, J. *et al.* High-contrast terahertz modulator based on extraordinary transmission through a ring aperture. *Opt. Express* **19**, 26666–26671 (2011).
35. Ordal, M. A. *et al.* Optical-properties of the metals Al, Co, Cu, Au, Fe, Pb, Ni, Pd, Pt, Ag, Ti, and W in the infrared and far infrared. *Appl. Opt.* **22**, 1099–1119 (1983).
36. Groner, M. D., Elam, J. W., Fabreguette, F. H. & George, S. M. Electrical characterization of thin Al<sub>2</sub>O<sub>3</sub> films grown by atomic layer deposition on silicon and various metal substrates. *Thin Solid Films* **413**, 186–197 (2002).

## Acknowledgments

This work was supported by the U.S. Department of Defense (DARPA Young Faculty Award N66001-11-1-4152; X.S.C., H.R.P., J.S., S.-H.O.). Device fabrication was performed at the University of Minnesota, Nanofabrication Center, which receives support from the National Science Foundation (NSF) through the National Nanotechnology Infrastructure Network program, and the Characterization Facility, which has received capital equipment funding from NSF through the Materials Research Science and Engineering Center. S.-H.O. also acknowledges support from the Office of Naval Research Young Investigator Award. X.S.C. acknowledges support from the 3M Science and Technology Fellowship and the University of Minnesota Doctoral Dissertation Fellowship.

## Author contributions

X.S.C., H.R.P. and S.-H.O. conceived and designed the experiments. X.S.C. fabricated all of the samples, and performed SEM and TEM analysis. H.R.P. constructed terahertz time-domain spectroscopy setup, measured terahertz transmission spectra, and produced SEM and photographs of devices. N.C.L. performed finite-element modeling. J.S. performed near-infrared spectroscopic measurements and data analysis. All authors analyzed the data and wrote the manuscript together.

## Additional information

**Competing financial interests:** The authors declare no competing financial interests.

**How to cite this article:** Chen, X. *et al.* Squeezing Millimeter Waves through a Single, Nanometer-wide, Centimeter-long Slit. *Sci. Rep.* **4**, 6722; DOI:10.1038/srep06722 (2014).



This work is licensed under a Creative Commons Attribution-NonCommercial-NoDerivs 4.0 International License. The images or other third party material in this article are included in the article's Creative Commons license, unless indicated otherwise in the credit line; if the material is not included under the Creative Commons license, users will need to obtain permission from the license holder in order to reproduce the material. To view a copy of this license, visit <http://creativecommons.org/licenses/by-nc-nd/4.0/>